Computer-Generated Holographic Beams for the Investigation of the Molecular and Circuit Function

Marco Dal Maschio

Abstract One of the goals of the modern research is to understand the signal processing and information propagation in biological systems clarifying the peculiar contribution of the different components in order to explore novel paradigms of computation and circuit wiring. For several years, the research in the field of neuroscience took advantage of a large set of fluorescence-based sensors to study the activity patterns ongoing in the neuronal circuits within the brain and the molecular mechanism underlying them. However, only recently, the advent of light-triggered molecular actuators has allowed a change in the research perspective moving the focus toward the investigation of the causal relations involved in the dynamics of the neuronal networks and in their function-optimized wiring. In parallel to the development of light-triggered molecules, scientists are looking for effective optical methods to increase the accuracy they could achieve by means of the light in the control of these tools and in the conditioning of the brain circuits. Moreover, the optical approaches, with respect to other investigation methods, are unique in allowing for a minimal-invasive investigation of the molecular mechanisms of the signal transduction underlying the cellular activity and the neuronal circuit function. In this perspective, computer-generated holographic beams, where the phase of the light wave front is controlled to obtain a specific light intensity distribution within the sample space, represent a parallel, dynamic, and powerful tool to investigate the molecular mechanism and the function of neuronal circuits.

M. Dal Maschio (✉)
Department of Neuroscience and Brain Technologies, Fondazione Istituto Italiano di Tecnologia, Genoa, Italy
e-mail: dalmaschio@neuro.mpg.de

M. Dal Maschio
Department of Genes, Circuits and Behavior, Max Planck Institute for Neurobiology, Martinsried, Germany

F. Benfenati et al. (eds.), *Novel Approaches for Single Molecule Activation and Detection*, Advances in Atom and Single Molecule Machines,
DOI: 10.1007/978-3-662-43367-6_2, © Springer-Verlag Berlin Heidelberg 2014

1 Introduction

Many optical techniques share the common property of being based on different methods for engineering the electric field distributions in the three-dimensional sample space to achieve specific illumination profiles. The generation of the doughnut-shaped intensity profile in stimulated emission depletion (STED) microscopy [1], the induction at the cell-substrate interface of an evanescent electric field in total internal reflection fluorescence (TIRF) [2, 3] or the enhancement of the near-field components in scanning near-field microscopy [4], the grating illumination patterns used for structured-illumination microscopy (SIM) [5], and the use of light sheets in low-scattering samples [6] are a few of the more clear examples. The optimization of the light distribution is usually leading per se or in combination with other cofactors to a significant enhancement of important figures in the signal detection such as the achievable optical resolution, the signal-to-noise ratio, the acquisition speed, the amount of accessible volume, or the number of accessible features of interest. The signals acquired from biological systems with these techniques come in most of the cases from specific labeling of molecules of interest, from synthetic or genetically encoded sensors of the cellular activity or of the molecular dynamics, and from reporters of the change in the cellular and extracellular environment, whose detection is based frequently on the excitation-emission properties of fluorescent moieties. Such fluorescent molecular tools allow for an extremely precise understanding of the cellular function and are continuously opening new windows in the characterization of the mechanisms underlying the brain circuits [7].

Optical methods in neuroscience, with the exception of the applications of the optical tweezers [8, 9], traditionally have been focused on the imaging aspects, in other words on monitoring the status of the sample in a short time interval or over a longer temporal range to characterize the changes induced by external stimuli. Until recently, optical methods for controlling molecular mechanisms and neuronal activity lagged behind methods for monitoring [10]. But, in the past few years, an impressive set of photochemical tools has become available to the purpose, including caged neurotransmitters, natural photosensitive proteins and small-molecule photoswitches introducing light sensitivity in ion channels and receptors [10]. Caged molecules are based on a photolabile protecting group, which when is removed upon light illumination liberate a bioactive compound. MNI-caged glutamate is now the most popular form of caged glutamate [11], with good 2P cross section and very low rate of spontaneous event in the dark. Caged versions for many other neurotransmitters have also been published for GABA [12] and anandamide [13]. On the group of natural photosensitive protein, ChR2 channel rhodopsin 2 [14], a light-sensitive cation channel from algae Chlamydomonas, is the most common example. In this kind of molecules, a trans to cis structural change in the chromophore induced by visible light absorption leads to a transient conformational rearrangement of the transmembrane protein, making it permeable to free ions and very suitable for a fine temporal control of the neuronal

activation [15]. Many other different types have been discovered either for excitation or for inhibition of neuronal firing [16]. More traditional examples of this class are the retinal photoreceptors, where rhodopsin and their associated proteins regulate ion channel activity through G protein biochemical cascade. The third class, the one named small-molecule photoswitches, includes tools rationally designed and synthetically manufactured to couple photosensitivity to non-intrinsically photosensitive ion channels or receptors. The photosensitivity is introduced by coupling a photoisomerizable molecule into ordinary channel in such a way that the light absorption induces the delivery or the removal of the ligand for the receptor binding site, thereby regulating its activity.

The most representative molecules of this group is the gated ionotropic glutamate receptor (LiGLuR) [17], based on glutamate derivative attached to an engineered kainite receptor via a tethered azobenzene photoisomerizable molecule.

Computer-generated holography (CGH) is one versatile method for the engineering of the light illumination pattern based on the modulation of the wave front phase. In combination with the different classes of optical actuators, this approach can allow for a spatial and temporal precise control of the molecule activity and brain circuit function. In this chapter will be first presented the basic optical principles behind the phase modulation scheme from the point of view of the light propagation theory. Then, the basic properties of the hardware aspects will be introduced starting from the core of the approach, the spatial light modulator (SLM), to the explanation of the different optical configurations achievable. Finally, an overview of the state of the art of the application of the method will be discussed.

2 Background and Computational Aspects in CGH

2.1 Computation of the Phase Maps

The propagation of a light from a source in the free space as within an optical system results in a light intensity distribution at the observation plane dictated by the interactions experienced by the light wave front with the different elements constituting the propagation medium. Such interactions are involving the properties of the electric field such as its amplitude and its phase. In CGH, the phase profile of the light wave front is carefully controlled in order to obtain at the observation plane a specific intensity distribution. From an optical point of view, the propagation of an arbitrary wave front can be considered as an envelope of spherical waves emitted from a point source (ξ, ζ) and moving in a certain direction. At the observation plane (x, y), the contribution of all the different waves is integrated to give an electrical field distribution $D(x, y)$ as expressed by

$$D(x,y) = \frac{1}{j\lambda} \iint\limits_{\sum} W(\xi,\zeta) \frac{e^{\mathrm{jkr}}}{r} cos\beta \mathrm{d}s$$

where $W(\xi, \zeta)\ e^{\mathrm{jkr}}$ is the single wave front component propagating from the source to the point (x, y) in the observation plane located to a distance r, β is the angle between the propagation direction z and the vector r, and k is the wave vector. From this equation, it is possible to derive, in the approximation at the second order for the vector r, a Fresnel diffraction integral in the following form

$$D(x,y) = \frac{e^{\mathrm{jkz}}}{j\lambda} e^{j\frac{k}{2z}\left(x^2+y^2\right)} \int_{-\infty}^{+\infty}\int W(\xi,\zeta)\left(e^{\frac{\mathrm{jk}}{2z}\left(\xi^2+\zeta^2\right)}\right)\left(e^{\frac{-j2\pi}{\lambda z}(x\xi+y\zeta)}\right)\mathrm{d}\xi\mathrm{d}\zeta$$

This form can be further reduced, considering a far-field approximation with the first term into the brackets substituted by 1. The field distribution in this case can be approximated by the Fraunhofer diffraction integral

$$D(x,y) = \frac{e^{\mathrm{jkz}}}{j\lambda} e^{j\frac{k}{2z}\left(x^2+y^2\right)} \int_{-\infty}^{+\infty}\int W(\xi,\zeta)\left(e^{\frac{-j2\pi}{\lambda z}(x\xi+y\zeta)}\right)\mathrm{d}\xi\mathrm{d}\zeta$$

This expression clearly shows that the electrical field distribution $D(x, y)$ obtained at the observation plane is, beside a quadratic phase factor, the two-dimensional Fourier transform of the complex field distribution $W(\xi, \zeta)$ at the source plane, linking amplitude and phase of the field at the observation plane to the component of the complex field at frequencies $(x/z, y/z)$ in the source plane. In other words, an input wave front can be modified in the phase of its spatial components in order to obtain upon propagation a specific light intensity distribution at the observation plane (Fig. 1).

In the application of the phase modulation in the light propagation scheme for CGH, the light intensity distribution at the observation plane $D(x, y)$ is an input parameter and finding the optimal field configuration at the source plane $W(\xi, \zeta)$ requires the use of mathematical algorithms and computation to retrieve the proper phase correction or diffractive optical element (DOE). Considering the last equation, in the condition with $W(\xi, \zeta)$ is a spatial uniform planar wave front, the propagation gives the definition of the Dirac delta, corresponding to a spot illuminated at the center of the observation plane. Similarly, introducing a correction of the wave front phase with a linear function of the position along one of the axis, i.e., $\varphi(\zeta) = \varepsilon\zeta \times 2\pi/\lambda z$, it leads to a lateral offset of the illumination spot of an amount proportional to ε and depending on the optical characteristics. These considerations are the basic blocks for a phase computation approach, known as gratings and lenses. This method [18], combines the optical properties of prisms to steer the light beam with those of the lenses to offset the illumination spot along

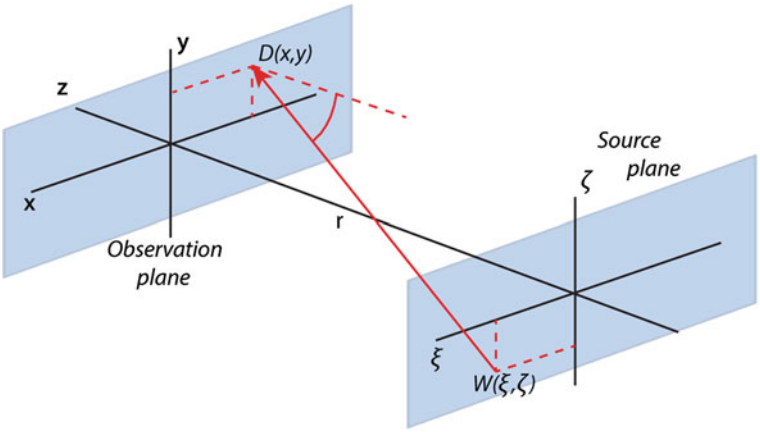

Fig. 1 Geometric representation of the optical conjugation between the source plane of a light beam and the observation or reconstruction plane where all the spatial components of the wave front are constructively or destructively contributing to the intensity distribution of the electric field and to the light intensity pattern

the optical axis. It is the simplest and computationally the fastest, because the required phase maps or diffractive optical elements (DOEs) can be obtained from the following analytical expression:

$$\varphi_{\text{grat}}(\xi,\zeta)+\varphi_{\text{lens}}(\xi,\zeta)=2\pi(\xi\Delta x+\zeta\Delta y)+\frac{2\pi\Delta f}{\lambda f^2}\left(\xi^2+\zeta^2\right)$$

where $\Delta x, \Delta y$, are the lateral offset values in the two directions of the observation plane, Δf is the desired step along the longitudinal direction z, and **f** is the effective focal distance of the system. This method can be easily extended to allow multiple beams to be generated in a volume and independently controlled by adding together the single field components at the source plane. For many applications, this approach is an effective method for DOE computation, but shaping capability is limited to ensembles of points only and the degree of longitudinal control is reduced by the far-field approximation [19]. A robust method to produce complex illumination patterns is the Gerchberg–Saxton [20] algorithm and the derived formulations. Compared to the gratings and lenses approach, where the phase are assigned and fixed for every spot in the pattern, this class of algorithm introduces phase freedom with an iterative optimization of the phase distribution at the DOE plane. The phase optimization procedure is based on the use of discrete Fourier transforms (DFT) to propagate the source field to the observation plane and to back-propagate the resulting complex field to the source plain again, imposing opportune constraints in the amplitude of the complex field.

The different implementations of these iterative Fourier transform algorithm (IFTA) share few common steps. Initially, from the DOE plane, a complex field

with uniform amplitude and random phase distributions is propagated by means of DFT. From the resulting field at the observation plane, the phase distribution is kept and the amplitude information replaced with the desired one. The new field is then back-propagated to the source plane by an inverse discrete Fourier transform. After the back-propagation, the amplitude of the field is replaced with the uniform pattern and the information phase retained to generate the complex field used in the following iteration. The convergence of this kind of algorithms is generally achieved in a few iterations. The original formulation of the GS algorithm has been successively expanded to essentially address two different aspects: the extension of the illumination patterns in the third dimension and the optimization of the uniformity in the light intensity distributions. Regarding the first point, it was demonstrated [21, 22] that the field in any plane of the observation space can be computed introducing a kernel in the field at the DOE and calculating the Fourier transform. This additional kernel represents the phase profile required to shift the plane of interest to the lens focal plane. This development allows for the generation in principle of extended illumination regions located at different plane in the image volume [23–25]. Regarding the research for higher uniformity, this has been motivated by the peculiar characteristic of the 2D-generated patterns to present a certain degree of intensity fluctuations. Specific algorithms have been developed, where, with respect to the original GS loop, more constraints are applied at the level of the observation plane to maximize the SNR of the generated pattern or a correction feedback accounting for the difference between the desired distribution and the one obtained is introduced to minimize the deviations.

3 Hardware for CGH: LCoS-SLM

3.1 LCoS-SLM: Working Principle

The common configuration to control the phase profile of a light wave front is based on nematic liquid-crystal-on-silicon spatial light modulators (LCoS-SLM). These devices are fabricated in the form of large bidimensional arrays typically covering an area of 16×12 mm^2 with 800×600 cells. The working principle of the SLM is based on the combination of the optical and dielectric properties of the liquid crystals (LC). From the structural point of view, these molecules are characterized by a uniaxial anisotropy, molecules with one main axis of symmetry called director and with two equal minor axes in the perpendicular directions giving them the particular physical properties. Depending on the relative angle θ of the light propagation direction with respect to the molecule orientation, the material presents an effective refraction index n_{eff} to the propagating radiation given by the following formula

$$n_{\text{eff}} = \frac{n_o n_e}{\sqrt{n_o^2 \cos^2\theta + n_e^2 \sin^2\theta}}$$

where n_o and n_e are respectively the ordinary and the extraordinary refractive indices experienced by an electrical field with polarization orientation perpendicular or along the director axis. The uniaxial anisotropy is reflected also in the dielectric properties of these materials that cause the LC to interact with an external electric field. The average direction of the molecules will orient as to align with the direction of the applied electric field, but because the rotation varies with the relative position within the thickness d of the LC layer, the effective refractive index experienced by the light traveling all the way in the material is given by the integral computed over the thickness interval. Because of the optical path change induced by the difference in the refraction index upon application of an electrical field, the portion of the wave front propagating along the direction z through this part of the material will experience a phase delay expressed in the following formula

$$\Gamma = \frac{2\pi}{\lambda} \int_0^d (n_{\text{eff}}(\theta(z)) - n_o) \mathrm{d}z$$

In general, the maximal phase stroke of the final device, in other words the amount of single-cell phase modulation in terms of π fractions, is dictated by the ratio between the cell thickness and the wavelength and is dependent on the material birefringence $\Delta n = n_e - n_o$ (Fig. 2).

Being the angular director distribution depending not exclusively on the external electric field applied to the cell but also on the elastic and viscous interactions affecting the LC molecules, the performance of these devices are generally a compromise between the LC responsiveness, dictating the actual refresh rate and reliability and precision in the phase modulation. At this purpose, theoretical frameworks like those described by Eriksen–Leslie theory [26, 27] are normally considered to characterize and to evaluate the dynamics of an LC compound when an electrical field is applied, according to the dynamic equation:

$$K_2 \frac{\partial^2 \vartheta}{\partial z^2} + \frac{\Delta \varepsilon E_z^2}{4\pi} \sin\vartheta \cos\vartheta = \gamma_1 \frac{\partial \vartheta}{\partial t}$$

where K_2 is the twist elastic coefficient, γ_1 is the rotational viscosity, Δε the dielectric anisotropy, and E_z is the amplitude of the applied electrical field. The approximated solutions to the linearized form of the equation are generally assumed to be a superposition of many spatial modes factorized in a temporal and a spatial term. The solution based on the first mode approximation, holding for small rotation angle, is extremely useful to highlight general features for the cell design and the selection of the LC material. In particular, the characteristic relaxation and settling times of the LC cell are proportional to the splay elastic

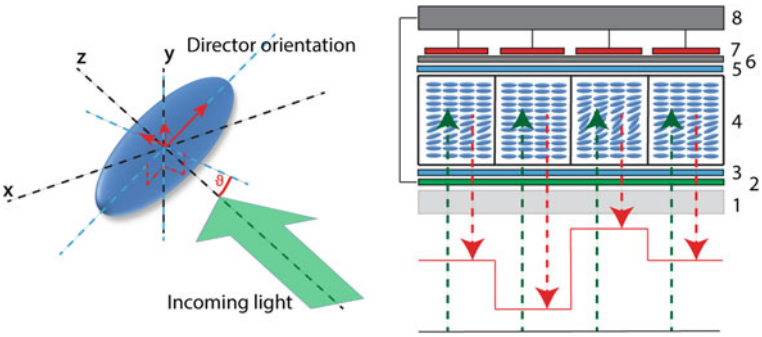

Fig. 2 **a** A schematic cartoon illustrating the spatial arrangement of LC molecules with respect to the light propagation direction and the profile these assume within an active cell of a spatial light modulator. **b** A simplified diagram of the SLM layout showing a set of cell (*4*) with different modulation profiles according to the control voltage applied by the electronic interface (*7* + *8*) and the change in the wave front superimposed to the propagating beam leaving the device

constant K_2, to the square of the cell thickness *d,* and to the viscosity coefficient of the material γ_1, according the following equations:

$$\tau_{\mathrm{OFF}} = \frac{\gamma_1}{K_2}\left(\frac{d}{\pi}\right)^2 \quad \text{and} \quad \tau_{\mathrm{ON}} = \frac{\gamma_1}{\Delta\varepsilon}\left(\frac{1}{E_z^2 - E_F^2}\right)$$

where E_F represents the threshold or Friedrich electric field. The performances and the modulation schemes achievable with SLM are not only depending on the intrinsic properties of the LC molecules but also depending on the overall design of the device and on configuration of the optical train build around it for the particular application.

3.2 LCoS-SLM: Temporal Features and Overdriving Procedures

The choice of the LC compound and the characteristic sizes of the active cell are fundamental parameters in the definition of the temporal response of device, and these factors should be carefully evaluated in the light of the envisaged application and modulation scheme. For instance, the ferroelectric LC have response times in the order of hundreds of microseconds leading to refresh rate of about 1 kHz, but are suitable for a binary phase modulation only resulting in SLMs with a lower diffraction efficiency compared to devices with an extended phase modulation resolution and thus limiting their utilization in applications where the light utilization efficiency is not the limiting factor. These figures of efficiency are enhanced in the case of devices with nematic LC but at the expense of the response times

that are falling down to the range of 5–50 ms due to the relatively higher viscosity characterizing this kind of molecules [28]. To improve the temporal performances for nematic LC devices, different approaches have been proposed and are continuously investigated. Along with the engineering of new LC blends [29] and of specific cell architectures [30, 31], a lot of efforts have been applied on the side of the LC electrical driving circuits and in overdriving techniques to minimize the effective response times. Generally, in the overdrive scheme [32], to speed up the transitions from different cell profiles corresponding to different phase values, the applied voltage to control the electric field across the cell is not simply switched from a level to the next one, but it is switched for an initial short time to the maximal or the minimal value allowed depending on the transition direction and only successively turned to the static level required for the next phase modulation once the cell configuration and the desired phase value has been achieved. Assuming an exponential response [33], the amount of time Δt during which the maximum or minimum voltage is applied depends on the phase difference between the transition states φ_0, φ_1 and the extreme phase modulation or phase stroke φ_m, and from the time constant τ required for switching the voltage between the minimum and the maximum values, according the following formula:

$$\Delta t(\varphi_0, \varphi_1) = -\tau \ln\left(\frac{\varphi_1 - \varphi_m}{\varphi_0 - \varphi_m}\right)$$

It is straightforward to realize that faster transitions are achieved when smaller phase jumps are considered. The performances of theses overdrive methods strongly depend on the maximum phase stroke achievable and the maximum driving voltage accepted, in particular in consideration of the fact that the maximum phase stroke is proportional to the cell thickness and that this one is affecting the temporal response in a quadratic dependence according to the approximated solutions of the models. Moreover, this approach assumes the use of control interfaces with refreshing times in the submillisecond range, significantly smaller with respect to the typical settling times of the LC cell.

3.3 LCoS-SLM: Design of the Device

In order to have a working phase modulation cell, the LC molecules need to be embedded in an optoelectronic functional unit able to manage at the same time the optical features of the material and the electrical circuit required for phase modulation. This is generally achieved with a structure including the following components: (1) an outer antireflection broadband or wavelength-specific protective glass layer; (2) a transparent ground electrode common to the all the cells made of indium tin oxide (ITO) coated with; (3) a SiO2 alignment layer to confer the proper orientation and pretilting angle to the LC molecules; (4) a layer of liquid crystal molecules; (5) an alignment matching layer; (6) a planar dielectric mirror to increase the effective fill

factor and to optimize the light utilization efficiency; and (7) a layer of evaporated Al pads.

The matrix of these functional units is matched to driving and addressing electronic circuits realized in complementary metal-oxide-semiconductor technology at very large integration scale (8).

On the market, there are many solutions available that mainly are differing for the LC material adopted, the alignment scheme, the number of the active elements in the SLM matrix, the feature size of the pixel, the electrical driving scheme of the LC cells, and the control interface. Typical matrix sizes are ranging from 256 × 256 to 1000 × 1900 elements with pixel diameters from 40 to 10 μm and active area of about 10 mm × 10 mm, resulting in spatial resolutions in the range of 20–33 lp/mm. All these parameters together contribute to define the temporal dynamics, the optical performances, and the modulation scheme of the devices.

3.4 LCoS-SLM: Optical Properties

One of the most important features of a SLM is its phase modulation characteristics, meaning the empirical relation between the voltage applied to the cell and the actual phase change produced. Depending on the working wavelength, the voltage applied to achieve a defined phase modulation, encoded with an 8-bit value, has to be calibrated according to a specific lookup table. These input–output characteristics can be obtained by interferometric methods or measuring the diffraction for binary linear gratings, or Ronchi gratings, with increasing phase modulation depth [34].

Another important figure for SLM is its diffraction efficiency η, defined as the ratio between the integrated intensity redirected in the first diffracted order and the intensity in the zero order due to the non-diffracted components of the light wave front. It strongly depends on the number of phase quantization levels q and the grating period Λ of the device according the following expression:

$$\eta = \frac{\sin c^2\left(\frac{1}{q}\right)}{\sin c^2\left(\frac{1}{[q,\Lambda]}\right)} \times \sin c^2\left(\frac{1}{\Lambda}\right)$$

where [ ] indicates the least common multiplier. Although the dependency in the quantization levels becomes quickly negligible increasing the quantization levels for the phase, the spatial discretization of the devices deriving from the pixelated structure of the matrix results in a non-uniform optical power density depending on the period of the diffraction grating. The method based on Ronchi gratings is less straightforward in the extrapolation of the LUT compared to interferometric methods, relaying in the measurement of the power addressed in the zero and first orders for the different modulations, but gives a more complete characterization of

the devices regarding its non-ideal behavior due to different kinds of phenomena such as edge effects, fringe field effects, back plate curvature, and non-uniformity. All these factors contribute in the reduction of the effective diffraction efficiency achievable. The pixel fill factor is also influencing the diffraction efficiency. Indeed, the regions between adjacent pixels of the device are without any control in the phase modulation, so increasing the amount of light contributing in the zero-order component. This contribution, in the case of the modern devices characterized by fill factors greater than 90 %, is hardly to be relevant.

4 Optical Configurations for CGH

4.1 Basic Configuration for CGH

The optical design required for CGH is essentially a Fourier holographic system, where the electric field at the output is given by the Fourier transformation of the electric field distribution at the input of the optical system realized with a single lens, with an objective or with a more elaborated optical path. In order to control the light intensity distribution at the focal volume of an objective, the phase correction map, superimposed by the SLM on the wave front of a propagating beam, has to be projected onto the objective back focal plane (Fig. 3).

In a basic optical setup, the coherent beam generated by a continuous wave or pulsed laser source is passed through an intensity modulation unit (MU), e.g., acousto-optic modulator or Pockell cell, in order to control the power density at the sample. Afterward, a half-wave plate to control the direction of the light polarization is generally placed to match the polarization requirement of the SLM for pure phase modulation dictated by the LC orientation. The original diameter of the beam successively is expanded by means of a telescope or commercial beam expander of 5x–10x factor in order to match the input window of the SLM that is illuminated at near-perpendicular incidence to preserve the optimal performances of the device while at the same time allowing for an easy lateral separation of the reflected beam. At this stage, in order to project the phase modulation map generated by the SLM onto the objective back focal plane of the imaging system, a telescope-based demagnification stage composed by lenses L1 and L2 is inserted along the path to generate a replica of the SLM screen properly fitting in the diameter of the objective back plane according to the following equations [35]:

$$mL_{\mathrm{SLM}} = 2 \times f_0 \times \mathrm{NA} \quad \text{and} \quad m = f_2/f_1$$

where m is the magnification factor of the telescope with L1 and L2 having focal lengths f_1 and f_2 respectively, f_0 is the focal length, NA the numerical aperture of the objective, and L_{SLM} is the size of the SLM. If the SLM image at the back aperture plane is smaller than the aperture diameter, the nominal NA of the

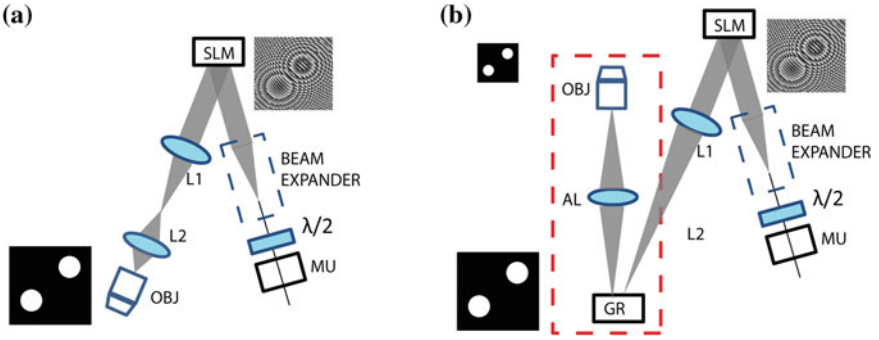

Fig. 3 Basic optical configuration for holographic projection **a** and its expansion to integrate the optical path for temporal focusing. At the SLM is superimposed to a propagating beam a proper phase correction map or diffractive optical element (DOE). At the Fourier-conjugated optical plane (between L1 and L2 in **a** and at the level of the grating GR in **b**), the desired intensity distribution is realized and demagnified at the sample plane

objective is not fully utilized with a consequent reduction in spatial resolution. On the other hand, with SLM image larger than the aperture, light efficiency is compromised.

4.2 Integration of CGH into Imaging Systems

Integration of a CGH optical train into an imaging system is very frequent and, depending on the implementation type, may require some degree of modification in the optical elements in particular when imaging and CGH designs are overlapping in the final segment of the microscope light path. The more common situations are represented by commercial infinity-corrected microscopes. In this case, a good approach is to couple the CGH path at the level of the fluorescence port between the objective and the tube lens. This approach, requiring a proper combining mirror in the microscope optical path and the telescope lenses mounted outside, is very versatile to combine in principle at the same time the phase modulation with other imaging techniques (Fig. 4).

A slight deviation from this scheme is achieved when the microscope tube lens serves as the second lens of the telescope required to image the SLM plane to the back focal plane of the objective. In this case, the integration is requiring minor hardware changes because the CGH path can be easily fed in through a secondary camera port in combination with a proper mirror but, on the other hand, leads to some implications on the CGH train design in terms of focal distances of the lenses and overall length of optical path. In principle, this last configuration compared to the original one allows for a more comfortable integration of the CGH module within a 2-photon or confocal scanning system. An alternative design [36–38] is

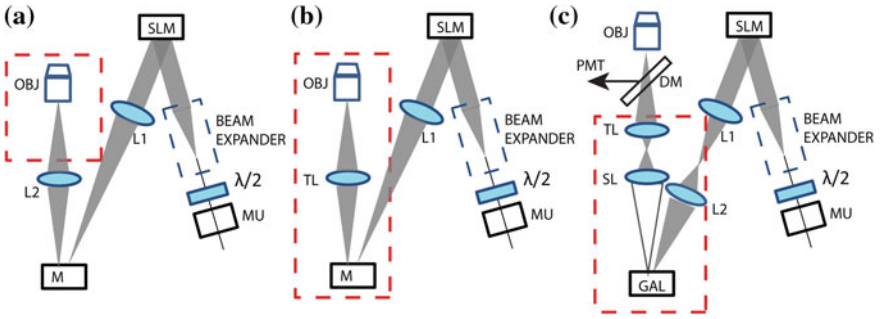

Fig. 4 Different integration schemes of CGH within imaging systems, almost independent optical trains in **a** where CGH shares with the imaging path only the segment after the lens L2; shared tube lens in **b**; configuration with scanning system in **c** with conjugation at the galvo mirror level

represented by the layout merging the CGH and the imaging paths within the scan head by means of a combining optic element placed before the scan lens. This configuration, being the magnification factor dictated by the tube and scan lenses in the last segment of the optical path, generally requires an additional magnification stage to project the SLM image into the plane of the galvo mirrors or to a plane located at the same distance from the scan lens.

4.3 Optical Figures of CGH

One of the optical aspects generally considered to characterize a CGH configuration is the size of the volume that can be addressed by means of the phase modulation, either in the transversal direction with respect to the direction of the light propagation or in the longitudinal direction when the reconstruction plane is shifted from the focal plane of the objective. The diameter of the excitation field in the transversal direction is a figure depending at the same time on the objective focal length f_0 and on the pixel size d_{SLM} of the SLM, on the basis of the following equations:

$$F_{\mathrm{MAX,TRANS}} = \frac{2 \times \lambda \times f_0}{n} \times \left(\frac{f_1}{f_2 d_{\mathrm{SLM}}} \right) = \frac{2 \times \lambda \times f_0}{n} \times \left(\frac{1}{m \times d_{\mathrm{SLM}}} \right)$$

where n is the refraction index of the medium. The second factor on the right side of the equation is representing the size of the pixel obtained at the back focal plane with the magnification performed by the telescope placed after the SLM. It is straightforward to realize that for a defined telescope configuration the addressable field is proportional to the objective focal length and inversely proportional to the size of the SLM pixel at the level of the back focal plane. The equation points also

to another important aspect of the optical configuration regarding the degree of filling of the SLM aperture. Indeed, underfilling SLM aperture assures for high light efficiency, but in order to match the condition for the maximum numerical aperture, the telescope magnification factor should be increased with consequent decrease of the size of the addressable field. On the other hand, with the overfilling, the minimal spot size is preserved at the expense of a slight reduction in the light utilization efficiency. Along with a transversal direction, the optical configuration for CGH gives the possibility to control the distribution of the electric field in a volume including the focal plane of the objective, with excitation foci located at different positions along the direction of light propagation [39, 40]. In this case, the longitudinal addressable range is limited by energy loss of rays coming from SLM pixel imaged at the periphery of the pupil. Pixels diffract light in a cone of half-angle in the order of $\lambda \times f_1 / (2 \times f_2 \times d_{\mathrm{SLM}})$, but compared to pixels located at the center of the pupil, those at the periphery can cover a smaller range of the optical axis. So with the axial defocus, progressively less energy is redirected from the peripheral pixels, limiting the effective axial range to about $\lambda \times f_0 \times n / (\mathrm{NA} \times m \times d_{\mathrm{SLM}})$.

The other important figure for a CGH system is the diffraction efficiency. Generally, the phase corrections leading to large displacement of illumination foci in the axial and lateral directions are characterized by high spatial frequencies. The discrete nature of the SLM renders these frequency components in a less accurate manner with respect to the low-frequency ones, leading to position-dependent diffraction efficiency. According to the Fraunhofer propagation theory [41], the diffraction efficiency η can be expressed in the case of a lateral displacement x, y with respect the center of the plane:

$$\eta(x,y) = \left(\sin c\left(\frac{\pi \mathrm{nm} d_{\mathrm{SLM}} x}{\lambda f_0}\right)\right)^2 \left(\sin c\left(\frac{\pi \mathrm{nm} d_{\mathrm{SLM}} y}{\lambda f_0}\right)\right)^2$$

This position-dependent diffraction efficiency leads to a non-uniform optical power at the sample and to an overall reduction of the power density over the addressable region. This scenario is further complicated in the case of combination of lateral and axial displacement.

4.4 Peculiar Aspects of CGH Beams for Bidimensional Extended Patterns

When CGH is adopted for the generation of extended regions of illumination in the observation space, the resulting intensity distributions present a few characteristic aspects. The first one is the evident intensity variability across the illuminated area. This phenomenon is mainly due to the cross talk between adjacent points of the plane of the DOE, which, having slightly different optical paths because of the

specific phase profile and the non-ideal properties of the overall optical system, sum up together randomly at the image plane, resulting in constructive or destructive mutual interference [42, 43]. This effect can lead to sensible fluctuations in the local intensity of the pattern, with values ranging from 30 to 60 % depending on the absorption mechanism of the excited molecules. Different methods have been adopted to minimize this variability in the applications requiring more uniform illumination profiles. The design of specific algorithms [44] is one approach based essentially on three different schemes: (1) imposing a constraint in the variation of the phase delay between adjacent pixels to smooth the phase profile [45]; (2) compute a set of DOEs including random phase patterns to mitigate the intensity fluctuation by time averaging [46]; and (3) with time averaging, but calculating a single DOE and then applying a procedure named cycling shifting to produce derived DOEs leading to field distributions at the image plane characterized by different phase profiles but sharing the same intensity distribution [47]. All these computational methods, although with different weight, have a common bottleneck in the computational time and load, limiting their application to relative slow experimental protocol or sophisticated computation platform. Other solutions have been proposed [48] based on the introduction along the optical path of a diffusing element to mitigate the beam coherency, but their potentiality cannot be adopted in those applications where light efficiency budget is critical.

A more severe aspect to carefully consider in CGH when generating two-dimensional patterns is the axial extension of the illumination profile along the direction of propagation of the light [49]. The relation of the axial extension to the lateral size of the projected illumination patter is linear and dictated by the rules of the diffraction [28]. This phenomenon leads to a relevant deterioration in the spatial resolution along the light propagation direction. This problem can be mitigated in the case of the 2-photon excitation, by means of temporal focusing [50]. With this method, an increase in the axial confinement of an extended illumination pattern is achieved controlling the dispersion of the pulse in such a way that the different spectral components are recombining effectively together only at the focal plane, while the pulse results dispersed in the regions out of focus. The hardware configuration is generally based on a grating to disperse the different chromatic components of the pulse at different angles and an achromatic lens forming with objective a perfect imaging system. In this way, a two-dimensional pattern projected to the grating is imaged at the sample plane at the same time with the spatial and the temporal focusing [51, 52].

5 Applications and Perspective for CGH

Over the last five years, the application of CGH method to shape the light illumination pattern has been used prevalently in combination with caged neurotransmitters. In 2008, the group of Emiliani [53] first demonstrated the possibility

of holographic photolysis of MNI-caged neurotransmitters in brain slices using a 405 nm laser source in combination with a SLM. Evident became the physiological implications in the study of neuronal activity and function deriving from the possibility to extend with the holographic beams the spatial and temporal features of the uncaging patterns in particular with respect to the traditional diffraction-limited point scanning approach. At the end of the same year, by the group of Yuste [36], the combination of spatial light modulators with a pulsed source was demonstrated in brain slices either applied for the simultaneous 2-photon uncaging of groups of dendritic spines with MNI glutamate or applied for a 2-photon parallel imaging approach of neuronal activity in cells loaded with the synthetic calcium indicator Fluo4 in acute brain slice based on the holographic excitation of large ensemble of points in combination with a CCD camera detection.

After the initial characterization of the performances of holographic MNI glutamate photostimulation based on electrophysiological recordings, the development moved toward the integration of the holographic shaping capabilities into systems for high-resolution functional imaging of the network activity. The clear goal was to develop an "all-optical" investigation system for triggering the network activation with high degree of control in the stimulation pattern in combination with the detection of the induced activity pattern using fluorescent probes for changes in calcium concentration. In particular, a CW holographic system [49] was presented for the stimulation of a set of cells in brain slice in combination with Hi-Lo, a widefield imaging scheme with improved depth discrimination to mitigate the tissue scattering. In the same period, an all-optical 2-photon configuration was presented in dal Maschio et al. [37]. In this work, a SLM-based holographic module was integrated within the scan head of a 2-photon imaging system equipped with two independent pulsed sources: one designed for the imaging and the other dedicated for the photostimulation. The engineered optical coupling was designed in order to have the possibility to use alternatively the SLM either for holographic uncaging while at the same time performing the imaging with the traditional scanning approach or to use the traditional diffraction-based uncaging done with the galvo mirror while imaging with a CCD camera and the parallel excitation scheme provided by the holographic beam.

At the end of the same year, the first demonstration of 2-photon excitation of Chr2 by means of wave front modulation approach was published by the Emiliani group [54]. The technique adopted in that case was the generalized phase-contrast GPC in combination with temporal focusing, where SLM is inserted in a common path interferometer and conjugated to the sample plane.

The possibility to use SLMs and the peculiar property of the holographic beams to design complex 3D light pattern was presented during the 2011 in three different works. Simultaneous generation of many uncaging spots at different depths within a brain slice was reported for the study of the integration property of dendritic processes [55, 56]. In dal Maschio et al. [38], it was presented a design to move the imaging focus plane in a 2P system along the light propagation direction without the movement of the objective but with the phase modulation approach. These

approaches demonstrated the effective possibility to decouple the imaging plane from the photostimulation plane.

Very recently, CGH beams have been used in combination with temporal focusing for the 2-photon photostimulation of a Chr2 variant, called C1V1, deep in the brain slice tissue [52]. In this study, the peculiar properties of temporal focusing in preserving the shape of the pattern within a scattering tissue were characterized.

In conclusion, only in the last 5 years, the efforts of many research groups led to the engineering effective of optical methods suitable for the investigation of the molecular function and of the dynamics of neuronal circuits. More time is required for the diffusion and the optimization of this kind of techniques, in particular for the application in vivo of these approaches.

References

1. Hell SW (2007) Far-field optical nanoscopy. Science 316(5828):1153–1158. doi:10.1126/science.1137395
2. Martin-Fernandez ML, Tynan CJ, Webb SE (2013) A 'pocket guide' to total internal reflection fluorescence. J Microsc 252(1):16–22. doi:10.1111/jmi.12070
3. Axelrod D, Thompson NL, Burghardt TP (1983) Total internal inflection fluorescent microscopy. J Microsc 29(Pt 1):19–28
4. Betzig E, Lewis A, Harootunian A, Isaacson M, Kratschmer E (1986) Development and biophysical applications. Biophys J 49(1):269–279
5. Aurélie J, Heintzmann R (2013) Superresolution multidimensional imaging with structured illumination microscopy. Annu Rev Mater Res 43:261–282. doi:10.1146/annurev-matsci-071312-121648
6. Santi PA (2011) Light sheet fluorescence microscopy: a review. J Histochem Cytochem 59(2):129–138. doi:10.1369/0022155410394857
7. Grewe BF, Langer D, Kasper H, Kampa BM, Helmchen F (2010) High-speed in vivo calcium imaging reveals neuronal network activity with near-millisecond precision. Nat Methods 7(5):399–405. doi:10.1038/nmeth.1453
8. Ashkin A, Dziedzic JM, Bjorkholm JE, Chu S (1986) Observation of a single-beam gradient force optical trap for dielectric particles. Opt Lett 11:288–290
9. Grier DG (2003) A revolution in optical manipulation. Nature 424:21–27. doi:10.1038/nature01935
10. Kramer RH, Fortin DL, Trauner D (2009) New photochemical tools for controlling neuronal activity. Curr Opin Neurobiol 19(5):544–552. doi:10.1016/j.conb.2009.09.004
11. Ellis-Davies GC (2007) Caged compounds: photorelease technology for control of cellular chemistry and physiology. Nat Methods 4(8):619–628. doi:10.1038/nmeth1072
12. Rial Verde EM, Zayat L, Etchenique R, Yuste R (2008) Photorelease of GABA with visible light using an inorganic caging group. Front Neural Circuits 13(2):2. doi:10.3389/neuro.04.002.2008
13. Heinbockel T, Brager DH, Reich CG, Zhao J, Muralidharan S, Alger BE, Kao JP (2005) Endocannabinoid signaling dynamics probed with optical tools. J Neurosci 25(41):9449–9459. doi:10.1523/JNEUROSCI.2078-05.2005
14. Nagel G, Szellas T, Huhn W, Kateriya S, Adeishvili N, Berthold P, Ollig D, Hegemann P, Bamberg E (2003) Channelrhodopsin-2, a directly light-gated cation-selective membrane channel. Proc Natl Acad Sci USA 100(24):13940–13945. doi:10.1073/pnas.1936192100

15. Zhang F, Wang LP, Brauner M, Liewald JF, Kay K, Watzke N, Wood PG, Bamberg E, Nagel G, Gottschalk A, Deisseroth K (2007) Multimodal fast optical interrogation of neural circuitry. Nature 446(7136):633–639. doi:10.1038/nature05744
16. Han X, Boyden ES (2007) Multiple-color optical activation, silencing, and desynchronization of neural activity, with single-spike temporal resolution. Plos One 212(3):e299. doi:10.1371/journal.pone.0000299
17. Volgraf M, Gorostiza P, Numano R, Kramer RH, Isacoff EY, Trauner D (2006) Allosteric control of an ionotropic glutamate receptor with an optical switch. Nat Chem Biol 2(1):47–52. doi:10.1038/nchembio756
18. Leach J, Wulff K, Sinclair G, Jordan P, Courtial J, Thomson L, Gibson G, Karunwi K, Cooper J, Laczik ZJ, Padgett M (2006) Interactive approach to optical tweezers control. Appl Opt 45(5):897–903. doi:10.1364/AO.45.000897
19. Yang S, Papagiakoumou E, Guillon M, de Sars V, Tang CM, Emiliani V (2011) Three-dimensional holographic photostimulation of the dendritic arbor. J Neural Eng 8(4):046002. doi:10.1088/1741-2560/8/4/046002
20. Gerchberg RW, Saxton WO (1972) A practical algorithm for the determination of the phase from image and diffraction plane pictures. Optik 35:237–246
21. Curtis JE, Koss BA, Grier DG (2002) Dynamic holographic optical tweezers. Opt Commun 207:169–175
22. Piestun R, Shamir J (1998) Generalized propagation-invariant wave fields. J Opt Soc Am A 15:3039–3044. doi:10.1364/JOSAA.15.003039
23. Sinclair G, Leach J, Jordan P, Gibson G, Yao E, Laczik Z, Padgett M, Courtial J (2004) Interactive application in holographic optical tweezers of a multi-plane Gerchberg–Saxton algorithm for three-dimensional light shaping. Opt Express 12(8):1665–1670. doi:10.1364/OPEX.12.001665
24. Whyte G, Courtial J (2005) Experimental demonstration of holographic three-dimensional light shaping using a Gerchberg–Saxton algorithm. New J Phys 7:117. doi:10.1088/1367-2630/7/1/117
25. Shabtay G (2003) Three-dimensional beam forming and Ewald's surfaces. Opt Commun 226(1–6):33–37. doi:10.1016/j.optcom.2003.07.056
26. Wu ST (1986) Phase retardation dependent optical response time of parallel-aligned liquid crystals. J Appl Phys 60:1836–1838. doi:10.1063/1.337228
27. Stewart I (2004) The static and dynamic continuum theory of liquid crystals: a mathematical introduction. Taylor and Francis, UK. ISBN:9780748408962
28. Oron D, Papagiakoumou E, Anselmi F, Emiliani V (2012) Two-photon optogenetics. Progress in brain research. In: Knöpfel T, Boyden E (eds) vol. 196. ISSN:0079-6123
29. Wu YH, Lin YH, Lu YQ, Ren H, Fan YH, Wu J, Wu ST (2004) Submillisecond response variable optical attenuator based on sheared polymer network liquid crystal. Opt Express 12(25):6382–6389. doi:10.1364/OPEX.12.006382
30. Wu ST, Wu CS (1989) High speed liquid crystal modulators using transient nematic effect. J Appl Phys 65:527. doi:10.1063/1.343135
31. Lin XW, Hu W, Hu XK, Liang X, Chen Y, Cui HQ, Zhu G, Li JN, Chigrinov V, Lu YQ (2012) Fast response dual-frequency liquid crystal switch with photo-patterned alignments. Opt Lett 37(17):3627–3629. doi:10.1364/OL.37.003627
32. Hu H, Hu L, Peng Z, Mu Q, Zhang X, Liu C, Xuan L (2012) Advanced single-frame overdriving for liquid-crystal spatial light modulators. Opt Lett 37(16):3324–3326. doi:10.1364/OL.37.003324
33. Thalhammer G, Bowman RW, Love GD, Padgett MJ, Ritsch-Marte M (2013) Speeding up liquid crystal SLMs using overdrive with phase change reduction. Opt Express 21(2):1779–1797. doi:10.1364/OE.21.00177
34. Zhang Z, Lu G, Francis TS (1994) Simple method for measuring phase modulation in liquid crystal televisions. Opt Eng 33:3018–3022
35. Pawley JB (ed) (2006) Handbook of biological confocal microscopy, 3rd edn. Springer, Berlin. ISBN 038725921X

36. Nikolenko V, Watson BO, Araya R, Woodruff A, Peterka DS, Yuste R (2008) SLM microscopy: scanless two-photon imaging and photostimulation with spatial light modulators. Front Neural Circuits 19(2):5. doi:10.3389/neuro.04.005
37. Dal Maschio M, De Stasi AM, Benfenati F, Fellin T (2011) Three-dimensional in vivo scanning microscopy with inertia-free focus control. Opt Lett 36(17):3503–3505. doi:10.1364/OL.36.003503
38. Dal Maschio M, Difato F, Beltramo R, Blau A, Benfenati F, Fellin T (2010) Simultaneous two-photon imaging and photo-stimulation with structured light illumination. Opt Express 18(18):18720–18731. doi:10.1364/OE.18.018720
39. Go MA, Stricker C, Redman S, Bachor HA, Daria VR (2012) Simultaneous multi-site two-photon photostimulation in three dimensions. J Biophotonics 5(10):745–753. doi:10.1002/jbio.201100101
40. Daria VR, Stricker C, Bowman R, Redman S (2009) Arbitrary multi-site two-photon excitation in four dimensions. Appl Phys Lett 95(9):093701–093703. doi: 10.1063/1.3216581. http://ieeexplore.ieee.org/search/searchresult.jsp?searchWithin=p_Authors:.QT.Bachor,%20H..QT.&searchWithin=p_Author_Ids:37283969400&newsearch=true
41. Golan L, Reutsky I, Farah N, Shoham S (2009) Design and characteristics of holographic neural photo-stimulation systems. J Neural Eng 6(6):066004. doi:10.1088/1741-2560/6/6/066004
42. Haupt C, Kolodziejczyk A, Tiziani HJ (1995) Resolution and intensity distribution of output images reconstructed by sampled computer-generated holograms. Appl Opt 34(17):3077–3086. doi:10.1364/AO.34.003077
43. Palima D, Gluckstad J (2008) Comparison of generalized phase contrast and computer generated holography for laser image projection. Opt Express 16:5338–5349. doi:10.1364/OE.16.005338
44. Golan L, Shoham S (2009) Speckle elimination using shift-averaging in high-rate holographic projection. Opt Express 17:1330–1339. doi:10.1364/OE.17.001330
45. Wyrowski F, Bryngdahl O (1988) Iterative Fourier-transform algorithm applied to computer holography. J Opt Soc Am A 5:1058–1065
46. Amako J, Miura H, Sonehara T (1995) Speckle-noise eduction on kinoform reconstruction using a phase-only spatial light modulator. Appl Opt 34(17):3165–3171. doi:10.1364/AO.34.003165
47. Matar S, Golan L, Shoham S (2011) Reduction of two-photon holographic speckle using shift-averaging. Opt Express 19(27):25891–25899. doi:10.1364/OE.19.025891
48. Papagiakoumou E, de Sars V, Emiliani V, Oron D (2009) Temporal focusing with spatially modulated excitation. Opt Express 17:5391–5401. doi:10.1364/OE.17.005391
49. Zahid M, Vélez-Fort M, Papagiakoumou E, Ventalon C, Angulo MC, Emiliani V (2010) Holographic photolysis for multiple cell stimulation in mouse hippocampal slices. PLoS One 5:e9431. doi:10.1371/journal.pone.0009431
50. Oron D, Tal E, Silberberg Y (2005) Scanningless depth-resolved microscopy. Opt Express 13:1468–1476. doi:10.1364/OPEX.13.001468
51. Papagiakoumou E, de Sars V, Oron D, Emiliani V (2008) Patterned two-photon illumination by spatiotemporal shaping of ultrashort pulses. Opt Express 16:22039–22047. doi:10.1364/OE.16.022039
52. Bègue A, Papagiakoumou E, Leshem B, Conti R, Enke L, Oron D, Emiliani V (2013) Two-photon excitation in scattering media by spatiotemporally shaped beams and their application in optogenetic stimulation. Biomed Opt Express 4(12):2869–2879. doi:10.1364/BOE.4.002869
53. Lutz C, Otis TS, DeSars V, Charpak S, David A, DiGregorio DA, Emiliani V (2008) Holographic photolysis of caged neurotransmitters. Nat Methods 5(9):821–827. doi:10.1038/nmeth.1241
54. Papagiakoumou E, Anselmi F, Begue A, de Sars V, Gluckstad J, Isacoff E, Emiliani V (2010) Scanless two-photon excitation of channelrhodopsin-2. Nat Methods 7:848–854. doi:10.1038/nmeth.1505

55. Anselmi F, Ventalon C, Bègue A, Ogden D, Emiliani V (2011) Three-dimensional imaging and photostimulation by remote-focusing and holographic light patterning. Proc Natl Acad Sci USA 108(49):19504–19509. doi:10.1073/pnas.1109111108
56. Yang S, Papagiakoumou E, Guillon M, de Sars V, Tang C, Emiliani V (2011) Three-dimensional holographic photostimulation of the dendritic arbor. J Neural Eng 8:046002. doi:10.1088/1741-2560/8/4/046002